



Micro-patterned cellulose films for flexible electrodes in medical implants

Mahyar Joodaki^a, Bert Müller^{a,b,*}, Helmut Schiff^c, Abinaya Nallathambi^a, Bekim Osmani^a

^a Biomaterials Science Center, Department of Biomedical Engineering, University of Basel, Gewerbstrasse 14, 4123 Allschwil, Switzerland

^b Biomaterials Science Center, Department of Clinical Research, University of Basel, 4031 Basel, Switzerland

^c Laboratory for Nano and Quantum Technologies, Paul Scherrer Institute (PSI), Forschungsstrasse 111, 5232 Villigen PSI, Switzerland

ARTICLE INFO

Keywords:

Silk-reinforced cellulose film
Gold adhesion via micro-pattern
Mechanical properties of cellulose films in phosphate buffer saline
Conductivity after cyclic loading

ABSTRACT

Neuromodulation treatments are based on the functional interface between the brain and man-made electrodes. Chronic inflammation around the implant, however, occurs as a result of mechanical mismatching between soft brain tissue and the stiff metallic electrode. After water uptake, cellulose films should prevent encapsulation of the electrode. In this work, we reinforced cellulose films with silk fibre networks, improving tear strength by a factor of four to seven and maintaining flexibility, characterised by an elastic modulus between 100 and 200 MPa. Whereas sputtered gold on flat films exhibited restricted adhesion, micro-patterning guaranteed reasonable adhesion of nanometre-thin gold to cellulose substrates. Micro-patterned cellulose films coated in 80 nm-thin gold retained conductivity for strains as large as 30%, while sheet resistance increased by a factor of about 30. Fabrication of the biocompatible electrodes is efficient and compatible with large-scale production.

1. Introduction

Substantial progress in neural interfaces have enabled the treatment of severe neurological diseases and disorders, as well as the study of neural network functionality through neuromodulation techniques [1]. Through neural interfaces, an electronic device can reconstruct impaired connectivity and collect signals relating to neural activity [1,2]. Non-invasive transcranial direct current stimulation has been applied to diagnose progressive neurodegenerative diseases, including Alzheimer's and Parkinson's, by employing local field potentials at low frequencies [3–5]. Recording extracellular action potentials, i.e. single-unit spikes, requires close proximity between electrodes and cells [6]. A prominent example in this regard is the treatment of leg paralysis or locomotor deficits caused by spinal cord injury [7].

Despite obvious progress, ensuring the efficiency of neural interfaces is still a challenging undertaking, due to mechanical mismatching between implants and tissue [8]. The elastic modulus E of grey and white matter has been reported at 1.9 and 1.4 kPa, respectively [9]. For peripheral nerves, (576 ± 160) kPa has been found [10]. The much harder neural probes cause local injuries, due to periodic micromovements leading to encapsulation and result in collapsing signals. Furthermore, corresponding stiffness makes the probes sensitive to buckling [11–13]. Future implants should therefore be compliant, in order to guarantee

glial scar-free neural-probe interfaces. Consequently, their long-term functioning under physiological conditions has to be tested [6,14,15]. Since the bending stiffness of a planar device scales cubically with its thickness and linearly with its elastic modulus [16], tailoring the device's geometry and elasticity is straightforward and suggested via twining electrodes [10], carbon-based fibre electrodes [17], mesh and Kirigami-structured devices [18,19]. Nevertheless, miniaturisation increases impedance and lowers signal quality, while pores in mesh structures limit electrode density [20].

Soft polymer-based probes can be flexible [21]. The limited adhesion of metals to polymers, as well as mechanical mismatching, however, causes cracks at desired strains. The mechanics of gold films on silicone leads to a network of cracks without a permanent loss of electrical conductivity after the strain is released [22]. Such cracks generally limit the lifetime of the devices. Nevertheless, conductive functionalised silicone [23] and two-dimensional interlayers [24] can substantially improve the adhesion of metal films to the polymer [25]. Moreover, it has been shown that the formation of a metal-polymer interphase improves bonding strength in thermoplastic applications [26,27]. Amorphous or hardly ordered polymers are better suited than crystalline ones [28,29]. It has already been shown that soft multichannel electrodes can be fabricated by depositing gold on thin bacterial cellulose [30].

Based on the state of the art, we fabricated a cellulose acetate

* Corresponding author at: Biomaterials Science Center, Department of Biomedical Engineering, University of Basel, Gewerbstrasse 14, 4123 Allschwil, Switzerland.

E-mail address: bert.mueller@unibas.ch (B. Müller).

<https://doi.org/10.1016/j.mne.2022.100162>

Received 28 February 2022; Received in revised form 7 July 2022; Accepted 30 July 2022

Available online 2 August 2022

2590-0072/© 2022 The Authors. Published by Elsevier B.V. This is an open access article under the CC BY license (<http://creativecommons.org/licenses/by/4.0/>).

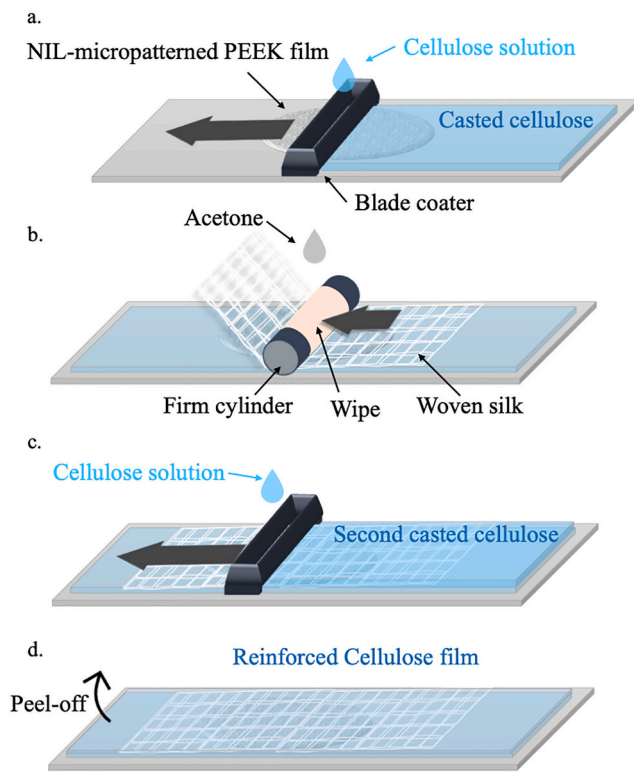


Fig. 1. Fabrication of the silk-reinforced micro-patterned cellulose film. **a.** Casting one layer of cellulose solution using a blade coater on top of an NIL-micro-patterned PEEK substrate. **b.** Embedding woven silk after evaporating the solvent, using droplets of acetone and a firm cylinder. **c.** Casting the second layer of the cellulose solution after evaporating acetone. **d.** Peeling off the reinforced film from the master PEEK substrate after solvent evaporation. Electron micrographs of the films after gold coating can be found in the supplementary material. (For interpretation of the references to colour in this figure legend, the reader is referred to the web version of this article.)

butyrate film reinforced with woven fabrics and deposited gold without an interlayer. These structures soften in a wet environment, thereby enabling the identification of a compliant interface with tissues of interest. We hypothesise that micro-patterning enhances gold adhesion to the required level. Cyclic loading under physiologically relevant conditions, i.e. in phosphate-buffered saline (PBS), should demonstrate the reliability of the microstructured devices developed herein.

2. Materials and methods

2.1. Fabrication of micro-patterned reinforced cellulose films

2.1.1. Preparation of the CAB solution

Cellulose acetate butyrate (CAB) belongs to commercially available non-toxic cellulose ester derivatives, known for their biocompatibility [31]. A longer butyrate branch improves flexural strength and elastic properties [32]. Thus, rather soft polymer films can be fabricated. In total, 200 g of cellulose acetate butyrate (CAB 500–5, 3 wt% acetyls, and 51 wt% butyryl and 1 wt% hydroxyl) with a glass transition temperature T_g of 96 °C (Eastman™ CAB, Eastman Chemical Company, USA) was dissolved in 800 g ethyl acetate (EtOAc) (> 99.5%, Carl Roth GmbH, Karlsruhe, Germany) and mixed for an hour. As a plasticiser, 100 g of bis (2-ethylhexyl) terephthalate ($\geq 96\%$, DOP, Sigma-Aldrich®, St. Louis, USA) with a molecular weight of 390.56 g/mol and density of 0.986 g/mL was added to the solution and mixed for another hour to obtain a uniform solution. A 30-min ultrasonic treatment followed, in order to prepare a bubble-free solution.

2.1.2. Preparation of the micro-patterned cellulose film, using blade-coating

Micro-patterns 800 nm deep, $25 \times 25 \mu\text{m}^2$ grating blocks with alternating orthogonal line patterns with a 4 μm pitch and periodic line patterns with feature sizes of 2 to 20 μm were printed on 75 μm -thick polyether ether ketone (PEEK) OPTIMA™ (Invibio® Biomaterial Solutions, Lancashire, UK) using thermal nanoimprint lithography (NIL) applying a precision hot press (HEX 03, Jenoptik AG, Jena, Germany) [33]. Using the micro-patterned PEEK, the cellulose film was formed while blade-coating the solution by employing a thickness of 0.5 mm and a speed of 0.3 mm/s. A 100 μm -thick cellulose film remained after solvent evaporation, as illustrated in Fig. 1(a).

2.1.3. Reinforcement of the carrier cellulose film and the deposition of gold

A piece of silk fabric (Fairy feather silk, SAIEI ORIMONO Co., LTD. /Saiei Silk, Fukushima, Japan) with a $(60 \pm 10) \mu\text{m}$ fibre diameter was embedded on the first layer of the cast cellulose film, using acetone. The second cellulose solution layer was coated on top of the silk, using a 0.5-mm blade-coater after evaporating the solvent, after about 15 min (see Fig. 1(b-d)). The 150 μm -thin micro-patterned film was peeled off after approximately half an hour. In order to reinforce the cellulose film with two layers of silk, the second layer of solution was coated by a 0.25 mm blade-coater. The process was repeated with silk fabric rotated by 45° with respect to the first layer. The final product with a total thickness of 200 μm was peeled off after the solvent evaporation.

In order to obtain a conductive film, gold (Au 99.99%, Sindlhauser Materials GmbH, Germany) was sputtered on the 0.2 mm-thick micro-patterned films at a current of 150 mA for a period of 40 s under an argon atmosphere (Q300TD, Quorum Technologies, Laughton, Great Britain).

2.2. Characterisation

The adhesion of the gold, with thicknesses ranging between 20 and 80 nm, to the cellulose was tested by a peel-off test using adhesive tape (Scotch® Magic™ Tape, 19 mm in width).

A universal testing machine (BOSE, ElectroForce3300, BOSE Corporation, New Castle, USA) served for mechanical analysis, see Fig. S1. We applied 1000 and 10,000 tensile-compression loading cycles for samples 0.1 mm thick and 25.6 mm long, using a sine waveform of 1 Hz frequency in PBS (Roti®-CELL PBS, CELLPURE® steril, Carl Roth GmbH, Germany), see Fig. S2. The displacement ranged from 2% tensile strain to a compression angle of 40°. The elastic modulus and tear strength were measured by applying opposite forces to both sides of the sample until they reached the fracture point for samples without and with scissor's pre-cut, respectively.

For electrical characterisation, four-point probe measurement was employed for the samples after cyclic loading under increasing tensile strain by means of a motorised translation stage (8MR200–100 STANDA LTD, Vilnius, Lithuania). Four liquid metal drops (Cool laboratory, Liquid Pro, Magdeburg, Germany) were placed on a strip of Au contact electrodes with a spacing s of 5 mm. Four semi-spherical probe tips (SPA-3 J, Everett Charles Technologies, Fontana, USA, by Distrelec AG, Nänikon, Switzerland) were mounted on micro-positioners (Signatone, APS Solution GmbH, Munich, Germany), and each was then lowered into contacting liquid metal droplets. A current I of 10^{-1} to $10^3 \mu\text{A}$ was applied to the outer probes and detected accordingly (Keithley 2401). Using a multimeter (Agilent 34461A Truevolt), voltage drop V between the inner probes was measured. Sheet resistance ρ of the gold film with a thickness d was calculated by [34].

$$\rho = \frac{V}{I} \frac{d}{s}$$

The morphology of the gold after each test was visualised by electron microscopy (EM-30AX^N, COXEM, Daejeon, Korea).

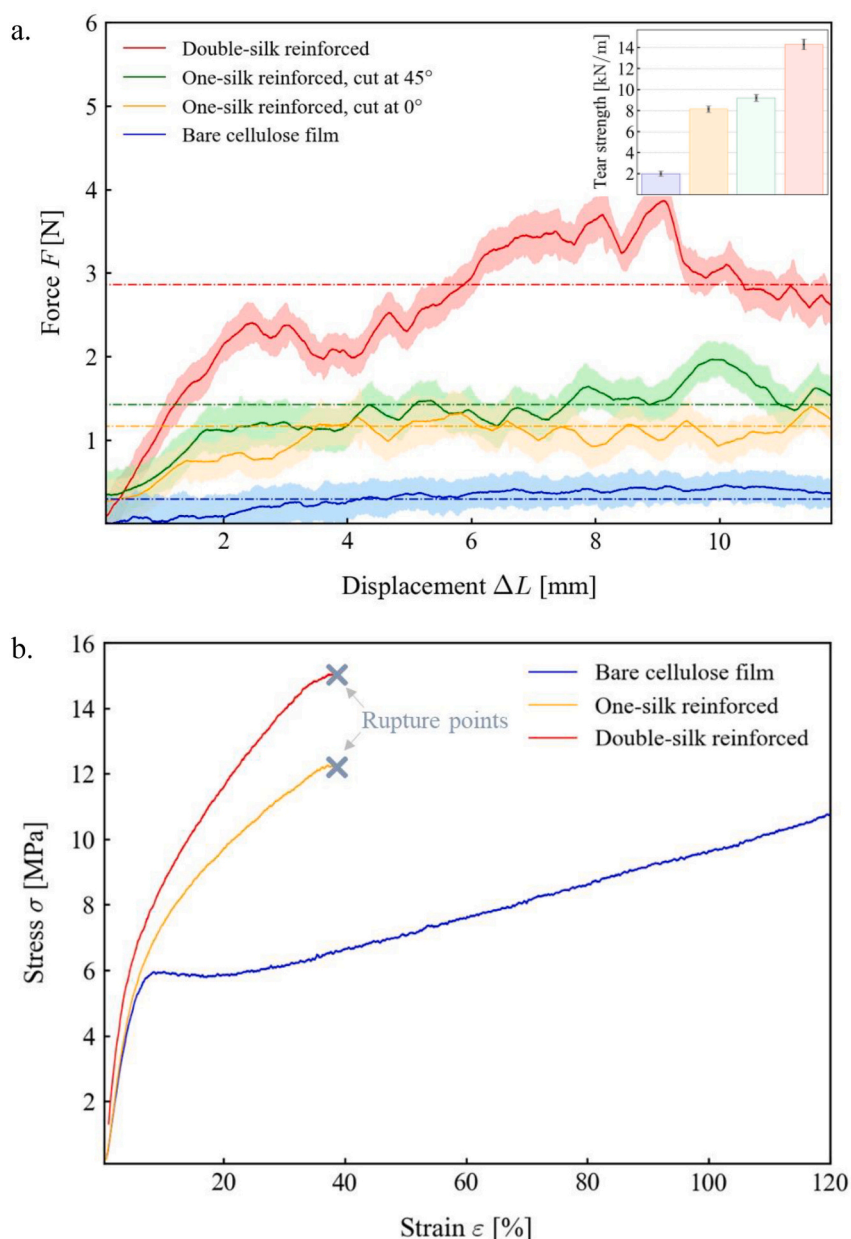


Fig. 2. The reinforcement of cellulose films augmented tear strength without substantial flexure change. a. The tear strength of cellulose films after one day in PBS. Solid lines, shadows and dash-dot lines show the average, standard deviation and mean value of applied force needed to tear the films, respectively. The mean forces determined were 0.30, 1.22, 1.38 and 2.86 N for bare and reinforced cellulose films. Tear strength values, see inset, could be increased through reinforcement by factors. b. Stress-strain curves for bare cellulose films (blue), one-layer (orange) and two-layer (red) silk-reinforced cellulose films. The slopes of the linear part, i. e. below 3% strain, correspond to their elastic moduli. For reinforced films, peak load corresponded to fracture. The softening stage seen for the bare cellulose film could not be attained [35].

3. Results

3.1. Mechanical analysis of the reinforced cellulose film

3.1.1. Tear strength measurements

Fig. 2 illustrates force-displacement relations for the bare and reinforced cellulose films embedded in PBS for one day. Silk reinforcement gave rise to a substantial increase in tear strength: single-layer silk enhanced tear strength by a factor of four to five, and double-layer silk increased it by more than a factor of seven with respect to the bare cellulose (see inset in Fig. 2a and Fig. S3).

3.1.2. Elastic modulus

The experimental stress-strain curves helped in determining the elastic moduli E and further relevant mechanical parameters. Before measurement, the films were placed in PBS for one day.

The bare cellulose films exhibited the behaviour of ductile plastic materials (see Fig. 2 (b), blue line). The reversible elastic behaviour could be related to $E = (124 \pm 7)$ MPa. Further tensile strain led to

plastic deformation with a yield strength σ_y of (4.33 ± 0.35) MPa. Breaking load was not reached because the machine was limited to a 120% strain.

The silk-reinforced cellulose films behaved like fabrics. Fracture tensile strain ε_u reached about 40%, as illustrated in Table 1. Whereas one layer of silk hardly affected the elastic modulus, the introduction of a second layer increased its value by almost 50%, see Fig. S4.

The actual start of plastic deformation could not be determined. Therefore, stress values σ_y were derived from the intersection of the straight line through the origin with slope E at a 0.2% strain. Ultimate tensile strength σ_u was given by stress at the elongation point [36].

Table 1 comparably lists the mechanical properties of the films. Whereas ductile properties were suppressed by silk reinforcement, yield strength and the elastic moduli of one-layer silk reinforced films barely changed.

3.2. Adhesion of gold on cellulose films

It can be reasonably expected that both the gold film thickness as

Table 1

Mechanical properties of bare and silk-reinforced cellulose films. The yield strength σ_y , elastic modulus E , ultimate strength σ_u and fracture strain (elongation) ϵ_u were extracted from stress-strain curves. The yield strength and fracture strain for the one-layer silk film were comparable to the two-layer silk-reinforced film, while the elastic modulus was well comparable to the bare film. The Young's moduli of polymers for neural implants (PDMS – polydimethylsiloxane, polyimide, parylene C – poly(p-xylylene), SU-8 - epoxy-based negative photoresist, LCP – liquid crystal polymer, BCB – benzocyclobutene) [37] are listed to highlight the softness of the cellulose films presented.

Cellulose film	Mechanical property			
	E (MPa)	ϵ_u (%)	σ_u (MPa)	σ_y (MPa)
Bare	124 ± 7	>120	> 10	4.33 ± 0.35
One-layer silk	131 ± 8	38 ± 2	12.27 ± 0.30	4.12 ± 0.43
Two-layer silk	183 ± 6	39 ± 2	15.10 ± 0.30	4.57 ± 0.36
PDMS	0.4–0.9			
Polyimide	2300–8500			
Parylene C	2760			
SU-8	2870–4400			
LCP	10,600			
BCB	3100			

well as the micro-structuring of the cellulose films will affect gold adhesion.

In a first series of experiments, a stripe pattern with periodicity changing from 4 to 20 μm with 20 and 40 nm gold on top was prepared and stored in air for few hours. After the peel-off test, electron micrographs enabled us to determine those regions with and without gold on a total area of $(8400 \pm 200) \mu\text{m}^2$ for each pattern restricted to the device's field of view, as shown in Fig. 3. The gold barely lifted from areas with pitches 4 and 6 μm wide. For the 20 μm -wide pitches and 40 nm gold thickness, coverage reduced to <60%, see Table 2.

A two-directional pattern with a minimum pitch size of 4 μm was chosen for testing adhesion for preselected Au film thicknesses. As listed in Table 3, for a nominal gold thickness of 20 nm, about 30% of gold was removed, whereas for thicknesses of 40 and 80 nm, areas without gold amounted to <1%. See Figs. S5 and S6 for further details.

3.3. Electrical properties of gold films on micro-structured cellulose films under loading

3.3.1. Tension-compression testing

Gold films with a nominal thickness of 80 nm on micro-structured cellulose were stored for one day and afterwards loaded in PBS - as schematically displayed in Fig. 4b. Their sheet resistance ρ was studied before loading and after 1000 and 10,000 loading cycles both in dry states. As shown by the electron micrographs in Fig. 4d, the degree of delamination depended on the selected micro-pattern. Surprisingly, sheet resistance remained in the same order of magnitude for the gold-

coated flat and two-dimensionally micro-patterned cellulose films, as illustrated in the bar diagram of Fig. 4e. Gold sputtered on the striped micro-structure given in Field 1 of Fig. 4 exhibited sheet resistance six orders of magnitude higher than the other ones. Gold on the two-dimensional micro-pattern, shown in Fields 2 and 3, seemed to have better interconnection and exhibited better adhesion than on the flat and striped cellulose films.

Because of water uptake from PBS, the cellulose films exhibited an increase in volume, for details see Table S1. The PBS-induced length increase of the bare cellulose film corresponded to $8.0\% \pm 0.6\%$, of the one-layer silk-reinforced film to $6.0\% \pm 0.6\%$, and of the two-layer silk-reinforced film to $2.0\% \pm 0.6\%$. Data acquired by electron microscopy, presented in Figs. S8 and S9, shows moderate impact on the film morphology. The micro-structure of Field 2 in Fig. 4 corresponds to the one represented in Figs. S8a/S8b and S9. The water-induced swelling is associated with softening. For example, comparing the Young's moduli of bare cellulose films kept for three days in air and water, respectively, one finds changes from (134 ± 8) to (104 ± 10) MPa.

3.3.2. Application of tensile and bending strain

Tensile strain was applied to gold-coated flat and micro-patterned bare cellulose films (cf. Field 2 in Fig. 4) in air environment as measuring electrical conductivity in PBS is impossible. Fig. 5a shows the sheet resistivity of the nominally 80 nm-thick gold film for eight pre-defined strain values. Whereas gold on the flat substrate only remained conductive up to 10% tensile strain, the gold film on the micro-patterned

Table 2

Gold coverage on one-dimensionally micro-patterned cellulose films after peel-off test. The coverage is >90% for 8 μm pitch size and below for the Au film thickness of 40 nm.

Pitch size (μm)	Gold coverage (%)
4	96.5 ± 3.1
6	98.5 ± 1.1
8	94.9 ± 2.4
10	88.4 ± 2.1
20	54.6 ± 3.8

Table 3

Gold coverage on two-dimensionally micro-patterned cellulose films with 4 μm pitch size after peel-off test. The coverage is >99% for 80 nm-thin gold films.

Au thickness (nm)	Gold coverage (%)
20	71.0 ± 4.6
40	97.0 ± 1.4
80	99.1 ± 0.9

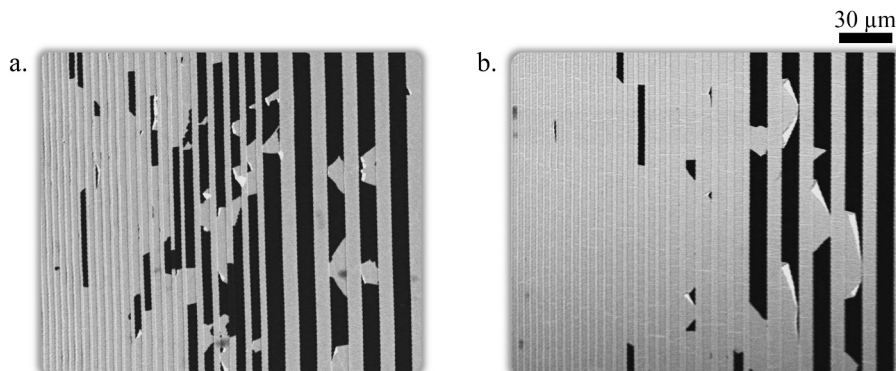


Fig. 3. To guarantee gold adhesion on micro-structured cellulose films, the pitch size has to be small enough. a and b. Electron micrographs after peel-off tests for a nominal gold thickness of 20 and 40 nm, respectively.

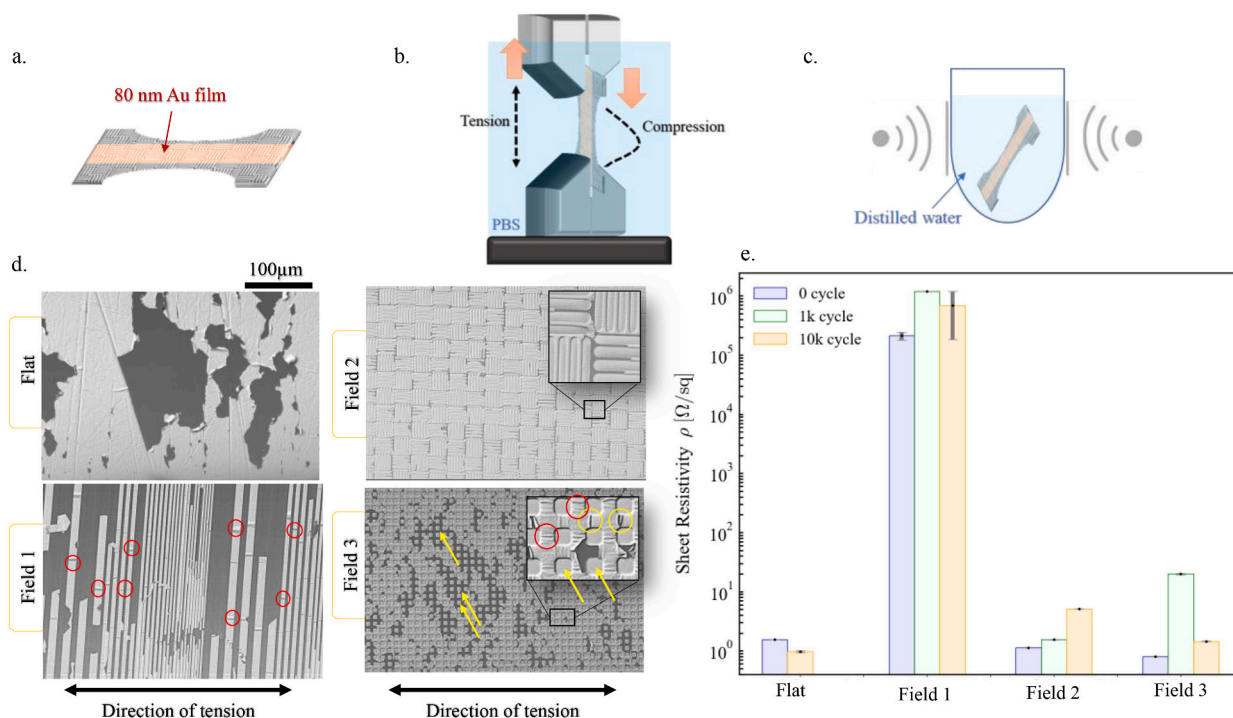


Fig. 4. Cycling tension-compression loading of gold-coated cellulose films resulted in micro-structure-dependent delamination but hardly impaired sheet resistivity ρ . Schematics of the experimental steps: **a.** 80 nm gold on micro-structured cellulose films; **b.** Tension-compression loading with $\theta = 41^\circ$, 2% strain at a frequency of 1 Hz frequency (sine wavefront in PBS); **c.** Cleaning in distilled water, using ultrasound for a period of 5 min; **d.** Electron micrographs obtained after 10,000 loading cycles with characteristic delamination defects indicated by red- and yellow-coloured circles (yellow arrows show gold adhesion in the valleys); **e.** Sheet resistivity ρ of films before (blue) and after 1000 (green) and 10,000 (orange) loading cycles.

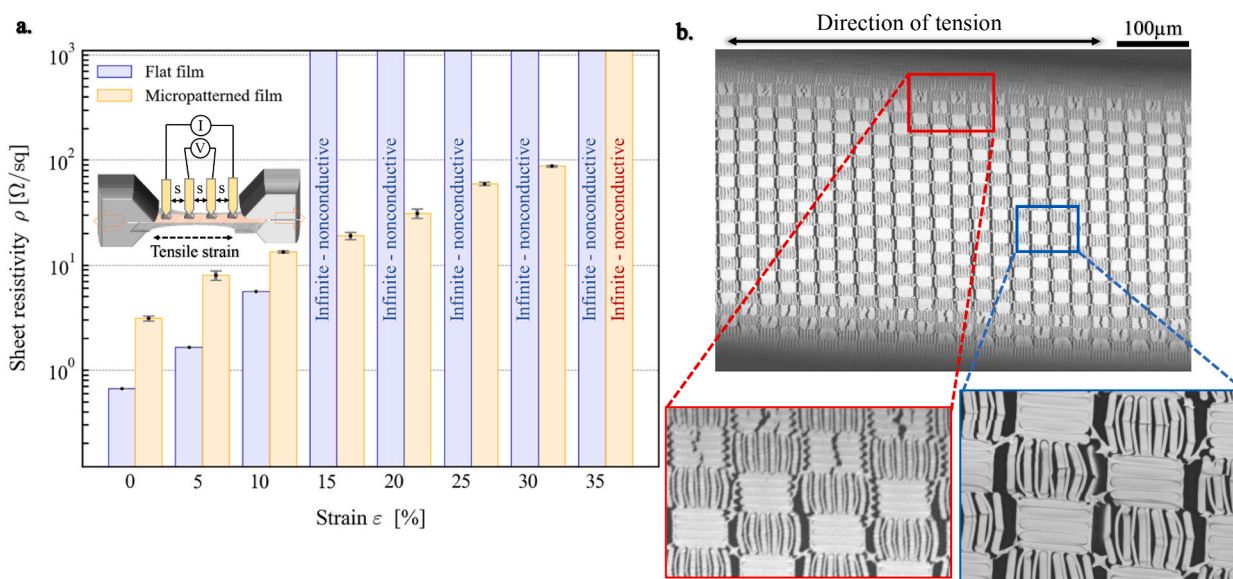


Fig. 5. Micro-structured electrodes remain conductive up to 30% tensile strain. **a.** Sheet resistivity for flat and micro-structured Au-coated cellulose films under 0 to 35% tensile strain. Inset: Schematic of four-probe measurements for the sample under tensile strain. Flat film (blue) remains conductive up to 10% of tensile strain, and it experiences electrical failure at 15% strain while micro-structured electrodes (orange) withstand up to 30% strain. **b.** Electron micrograph of a micropatterned (grating blocks) electrode for Field 2 after tensile testing up to 30% of tensile strain ϵ_t with 240 times magnification.

cellulose withstood tensile strains as high as 30%. The electron micrograph obtained after applying 30% tensile strain is represented in Fig. 5b. Connections between the elements of the pattern were retained despite the formation of cracks. This information is in line with bending experiments. At bending strains of up to 16%, gold film on the flat cellulose substrate displayed numerous cracks and associated delamination, whereas micro-patterning suppressed the delamination and

debonding of the gold from the cellulose films (see Fig. S7).

4. Discussion

Soft, transparent and ductile cellulose films were prepared. Their elastic modulus of (124 ± 7) MPa was about half of the value reported in the literature [38], while the fracture strain was higher than 120%.

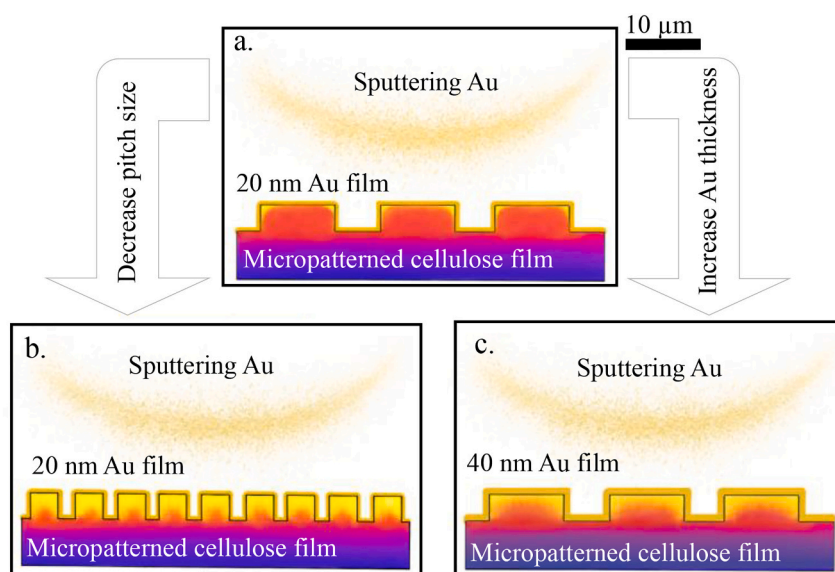


Fig. 6. Reaching the T_g of cellulose films during the sputtering of electrodes hypothesised as the parameter contributes to improving the adhesion of metal-polymer films. a-c. Schematics of the temperature gradient on the surface of cellulose films during the sputtering of Au film with preselected thicknesses.

Their tear strength, however, at 2 kN/m was inadequately low. Reinforcement by one-layer or even double-layer silk improved the films' resistivity against tearing by a number of factors while also keeping elasticity almost constant. Importantly, the reinforced films fractured at tensile strains beyond 38%, a value much higher than critical for neural implant [39]. The stiffness of the silk-reinforced cellulose can be simply tailored by adapting thickness.

The cellulose applied to realize films exhibits a Young's modulus, which is about one order of magnitude lower than most of the relevant polymers for neural implants, see Table 1. Thus, the mechanical mismatch between the physically soft human tissue and the electrode material is substantially reduced. The mismatch becomes even smaller by the water uptake of cellulose.

Polydimethylsiloxane (PDMS) is more than two orders of magnitude softer than the cellulose applied in this study [37]. Its handling for surgical procedures, however, is challenging and generally incompatible with minimally invasive procedures. Consequently, the use of silk-reinforced cellulose with a Young's modulus between 100 and 200 MPa is a reasonable trade-off for applications in neural implants.

Micro-patterned PEEK as a flexible intermediate stamp for cellulose allowed for not only thermal nanoimprint preparation, but also for facile removal because of inherently low adhesion. Reusage of the PEEK template also became possible.

Micro-patterning substantially improved the adhesion of the nanometre-thin gold layer to the cellulose substrates. Two-dimensional micro-patterns are superior to one-dimensional microstructures, a phenomenon which can be explained via the increased contact area between gold and cellulose. We hypothesise that this was not the only effect, though, as the glass transition temperature of 96 °C is an important feature [40]. Whilst sputtering, the polymer surface might have reached this temperature, which could have been reduced by the plasticiser we used. The smaller the pitch size and the longer the sputtering time, the higher the probability of reaching the glass transition temperature (note limited heat conductivity at the polymer edges). Beyond the glass transition temperature, the metal clusters could be integrated into the polymer and enhance adhesion (see Fig. 6).

Although cracks in the nanometre-thin gold film on the flat cellulose substrate were formed at bending strengths of 4.5%, the film remained conductive up to a 10% tensile strain, which is higher than the reported fracture toughness of 5% for gold films and almost independent of its thickness [41,42]. It should be noted that although a substantial part of

gold on flat films delaminated, some gold islands are connected, as indicated by the micrograph in Fig. 4d, resulting in reasonable electrical conductivity for the flat films, see bar diagram in Fig. 4e. Gold sputtered on two-dimensionally micro-patterned cellulose substrates barely formed cracks at the relevant strains. The layered structures remained conductive up to a 30% strain associated with a rise of less than one order of magnitude in sheet resistivity. The electron micrographs showed severe damage after mechanical loading. Conductivity, however, was maintained as a result of gold filaments connecting the blocks at the corners. This pattern could be employed as a mesh framework. The 30% strain corresponds to a bending radius of about 66 μm when considering a 100 μm -thin structure. The related curvature is 15 mm^{-1} and therefore 30 times larger than needed for targeted anatomical features in human brain [43]. Even conformable thin-film arrays can be built applying micrometre-thin substrates of non-stretchable materials, as their thickness is properly tailored to the curvature of the target structure [44].

Contrary to the earlier study combining bioresorbable substrates of silk fibroin with gold [19], the woven silk used in this study is not dissolvable within the body. The present study used silk for reinforcement of the cellulose films they have been embedded into.

It should be highlighted that surface topology modifications, for example tailored via thermal imprinting of cellulose to generate dedicated micro-pattern, can positively influence the morphology and outgrowth of nerve and neuroglial cells [45].

5. Conclusion

As a result of water uptake, cellulose films soften and can alter the curvature of anatomical features in the brain and spine. These films, however, could be silk-reinforced to substantially improve their mechanical properties and retain flexibility. Two-directional micro-structures imprinted on the cellulose considerably improved the adhesion of sputtered gold films, which remained conductive beyond a 30% strain. Consequently, nanometre-thin gold layers on micro-structured, silk-reinforced cellulose films are expected to become compliant electrodes for next-generation neural implants in brain and peripheral nerves.

Declaration of Competing Interest

The authors declare that they have no known competing financial

interests or personal relationships that could have appeared to influence the work reported in this paper.

Acknowledgments

The financial support of the Gebert Rüf Foundation, Switzerland, Grant-ID GRS-058/18, is gratefully acknowledged. The authors wish to thank Konrad Vogelsang very much for his technical assistance with the thermal imprinting of the PEEK substrates. The authors would also like to thank Sascha Martin from the mechanical workshop at the Department of Physics, University of Basel, for preparing the saline bath for the cyclic loading measurements.

Appendix A. Supplementary data

Supplementary data to this article can be found online at <https://doi.org/10.1016/j.mne.2022.100162>.

References

- [1] M. Zhang, Z. Tang, X. Liu, J. Van der Spiegel, Electronic neural interfaces, *Nat. Electron.* 3 (4) (Apr. 2020) 191–200, <https://doi.org/10.1038/s41928-020-0390-3>.
- [2] E. Song, J. Li, S.M. Won, W. Bai, J.A. Rogers, Materials for flexible bioelectronic systems as chronic neural interfaces, *Nat. Mater.* 19 (6) (Jun. 2020), <https://doi.org/10.1038/s41563-020-0679-7>. Art. no. 6.
- [3] D. Aloï, A.I. Della Rocchetta, A. Ditchfield, S. Coulborn, D. Fernández-Espejo, Therapeutic use of transcranial direct current stimulation in the rehabilitation of prolonged disorders of consciousness, *Front. Neurol.* 12 (2021) 442, <https://doi.org/10.3389/fneur.2021.632572>.
- [4] Y. Luo, et al., Anodal transcranial direct current stimulation can improve spatial learning and memory and attenuate A β 42 burden at the early stage of Alzheimer's disease in APP/PS1 transgenic mice, *Front. Aging Neurosci.* 12 (2020) 134, <https://doi.org/10.3389/fnagi.2020.00134>.
- [5] F. Pol, M.A. Salehinejad, H. Baharlouei, M.A. Nitsche, The effects of transcranial direct current stimulation on gait in patients with Parkinson's disease: a systematic review, *Trans. Neurodegen.* 10 (1) (Jun. 2021) 22, <https://doi.org/10.1186/s40035-021-00245-2>.
- [6] F. He, R. Lycke, M. Ganji, C. Xie, L. Luan, Ultraflexible neural electrodes for long-lasting intracortical recording, *iScience* 23 (8) (Aug. 2020) 101387, <https://doi.org/10.1016/j.isci.2020.101387>.
- [7] F.B. Wagner, et al., Targeted neurotechnology restores walking in humans with spinal cord injury, *Nature* 563 (7729) (Nov. 2018) 65–71, <https://doi.org/10.1038/s41586-018-0649-2>.
- [8] H. Acarón Ledesma, X. Li, J.L. Carvalho-de-Souza, W. Wei, F. Bezanilla, B. Tian, An atlas of nano-enabled neural interfaces, *Nat. Nanotechnol.* 14 (7) (Jul. 2019) 645–657, <https://doi.org/10.1038/s41565-019-0487-x>.
- [9] S. Budday, et al., Mechanical properties of gray and white matter brain tissue by indentation, *J. Mech. Behav. Biomed. Mater.* 46 (Jun. 2015) 318–330, <https://doi.org/10.1016/j.jmbmm.2015.02.024>.
- [10] G.H. Borschel, K.F. Kia, W.M. Kuzon, R.G. Dennis, Mechanical properties of acellular peripheral nerve, *J. Surg. Res.* 114 (2) (Oct. 2003) 133–139, [https://doi.org/10.1016/S0022-4804\(03\)00255-5](https://doi.org/10.1016/S0022-4804(03)00255-5).
- [11] S. Guan, et al., Elastocapillary self-assembled neurotassels for stable neural activity recordings, *Sci. Adv.* 5 (3) (Mar. 2019) eaav2842, <https://doi.org/10.1126/sciadv.aav2842>.
- [12] A. Canales, et al., Multifunctional fibers for simultaneous optical, electrical and chemical interrogation of neural circuits in vivo, *Nat. Biotechnol.* 33 (3) (Mar. 2015) 277–284, <https://doi.org/10.1038/nbt.3093>.
- [13] L. Luan, et al., Ultraflexible nanoelectronic probes form reliable, glial scar-free neural integration, *Sci. Adv.* 3 (2) (Feb. 2017) e1601966, <https://doi.org/10.1126/sciadv.1601966>.
- [14] G. Guitchounts, J.E. Markowitz, W.A. Liberti, T.J. Gardner, A carbon-fiber electrode array for long-term neural recording, *J. Neural Eng.* 10 (4) (Aug. 2013) 046016, <https://doi.org/10.1088/1741-2560/10/4/046016>.
- [15] J. Liu, et al., Syringe-injectable electronics, *Nat. Nanotechnol.* 10 (7) (Jul. 2015) 629–636, <https://doi.org/10.1038/nnano.2015.115>.
- [16] Z. Suo, E.Y. Ma, H. Gleskova, S. Wagner, Mechanics of rollable and foldable film-on-foil electronics, *Appl. Phys. Lett.* 74 (8) (Feb. 1999) 1177–1179, <https://doi.org/10.1063/1.123478>.
- [17] T.D.Y. Kozai, et al., Ultrasmall implantable composite microelectrodes with bioactive surfaces for chronic neural interfaces, *Nat. Mater.* 11 (12) (Dec. 2012) 1065–1073, <https://doi.org/10.1038/nmat3468>.
- [18] Y. Morikawa, et al., Ultrastretchable Kirigami bioprobes, *Adv. Healthcare Mater.* 7 (3) (2018) 1701100, <https://doi.org/10.1002/adhm.201701100>.
- [19] D.-H. Kim, et al., Dissolvable films of silk fibroin for ultrathin, conformal bio-integrated electronics, *Nat. Mater.* 9 (6) (Jun. 2010) 511–517, <https://doi.org/10.1038/nmat2745>.
- [20] M. Lee, H.J. Shim, C. Choi, D.-H. Kim, Soft high-resolution neural interfacing probes: materials and design approaches, *Nano Lett.* 19 (5) (May 2019) 2741–2749, <https://doi.org/10.1021/acs.nanolett.8b04895>.
- [21] K.M. Szostak, L. Grand, T.G. Constandinou, Neural interfaces for Intracortical recording: requirements, fabrication methods, and characteristics, *Front. Neurosci.* 11 (2017) 665, <https://doi.org/10.3389/fnins.2017.00665>.
- [22] M.A. McClain, I.P. Clements, R.H. Shafer, R.V. Bellamkonda, M.C. LaPlaca, M. G. Allen, Highly-compliant, microcable neuroelectrodes fabricated from thin-film gold and PDMS, *Biomed. Microdevices* 13 (2) (Apr. 2011) 361–373, <https://doi.org/10.1007/s10544-010-9505-3>.
- [23] B. Osmani, T. Töpfer, M. Siketanc, G.M. Kovacs, B. Müller, Electrospinning and ultraviolet light curing of nanometer-thin polydimethylsiloxane membranes for low-voltage dielectric elastomer transducers, in: *Electroactive Polymer Actuators and Devices (EAPAD) 2017* 10163, Apr. 2017, p. 101631E, <https://doi.org/10.1117/12.2258214>.
- [24] C. Cho, et al., Strain-resilient electrical functionality in thin-film metal electrodes using two-dimensional interlayers, *Nat. Electron.* 4 (2) (Feb. 2021) 126–133, <https://doi.org/10.1038/s41928-021-00538-4>.
- [25] B. Moazzez, S.M. O'Brien, E.F. Merschrod S, Improved adhesion of gold thin films evaporated on polymer resin: applications for sensing surfaces and MEMS, *Sensors* 13 (6) (Jun. 2013), <https://doi.org/10.3390/s130607021>. Art. no. 6.
- [26] L.-H. Lee, Molecular bonding and adhesion at polymer-metal interphases, *J. Adhes.* 46 (1–4) (Sep. 1994) 15–38, <https://doi.org/10.1080/00218469408026646>.
- [27] L. Chu, et al., Influence of the polymer interphase structure on the interaction between metal and Semicrystalline thermoplastics, *Adv. Eng. Mater.* 23 (2) (2021) 2000518, <https://doi.org/10.1002/adem.202000518>.
- [28] J. Karger-Kocsis, Interphase with lamellar interlocking and amorphous adherent – a model to explain effects of Transcrystallinity, *Adv. Compos. Lett.* 9 (3) (May 2000), <https://doi.org/10.1177/096369350000900307>, p. 096369350000900307.
- [29] W. Xia, X. Qin, Y. Zhang, R. Sinko, S. Keten, Achieving enhanced interfacial adhesion and dispersion in cellulose nanocomposites via amorphous interfaces, *Macromolecules* 51 (24) (Dec. 2018) 10304–10311, <https://doi.org/10.1021/acs.macromol.8b02243>.
- [30] J. Yang, et al., Bacterial cellulose as a Supersoft neural interfacing substrate, *ACS Appl. Mater. Interfaces* 10 (39) (Oct. 2018) 33049–33059, <https://doi.org/10.1021/acsami.8b12083>.
- [31] C. Huang, H. Niu, C. Wu, Q. Ke, X. Mo, T. Lin, Disc-electrospun cellulose acetate butyrate nanofibers show enhanced cellular growth performances, *J. Biomed. Mater. Res. A* 101A (1) (2013) 115–122, <https://doi.org/10.1002/jbm.a.34306>.
- [32] J. Dou, A. Karakoç, L.-S. Johansson, S. Hietala, D. Evtuygin, T. Vuorinen, Mild alkaline separation of fiber bundles from eucalyptus bark and their composites with cellulose acetate butyrate, *Ind. Crop. Prod.* 165 (Jul. 2021) 113436, <https://doi.org/10.1016/j.indcrop.2021.113436>.
- [33] B. Osmani, et al., Hierarchically structured polydimethylsiloxane films for ultra-soft neural interfaces, *Micro Nano Eng.* 7 (Jun. 2020) 100051, <https://doi.org/10.1016/j.mne.2020.100051>.
- [34] BSTJ 37: 3. May 1958, Measurement of Sheet Resistivities with the Four-Point Probe. (Smits, F.M.), Accessed: Jul. 19, 2021. [Online]. Available: <http://archive.org/details/bstj37-3-711>, 1958.
- [35] V.D. Truong, D.J. Kim, A review paper on direct tensile behavior and test methods of textile reinforced cementitious composites, *Compos. Struct.* 263 (May 2021) 113661, <https://doi.org/10.1016/j.compstruct.2021.113661>.
- [36] H.-P. Zhao, X.-Q. Feng, H.-J. Shi, Variability in mechanical properties of Bombyx mori silk, *Mater. Sci. Eng. C* 27 (4) (May 2007) 675–683, <https://doi.org/10.1016/j.msec.2006.06.031>.
- [37] A. Weltman, J. Yoo, E. Meng, Flexible, penetrating brain probes enabled by advances in polymer microfabrication, *Micromachines* (Basel) 7 (10) (Oct. 2016) E180, <https://doi.org/10.3390/mi7100180>.
- [38] A. Baltazar-y-Jimenez, M. Bistriz, E. Schulz, A. Bismarck, Atmospheric air pressure plasma treatment of lignocellulosic fibres: impact on mechanical properties and adhesion to cellulose acetate butyrate, *Compos. Sci. Technol.* 68 (1) (Jan. 2008) 215–227, <https://doi.org/10.1016/j.compscitech.2007.04.028>.
- [39] A. Sridharan, J.K. Nguyen, J.R. Capadona, J. Muthuswamy, Compliant intracortical implants reduce strains and strain rates in brain tissue in vivo, *J. Neural Eng.* 12 (3) (Jun. 2015) 036002, <https://doi.org/10.1088/1741-2560/12/3/036002>.
- [40] V. Zaporojtchenko, T. Strunskus, J. Erichsen, F. Faupel, Embedding of noble metal nanoclusters into polymers as a potential probe of the surface glass transition, *Macromolecules* 34 (5) (Feb. 2001) 1125–1127, <https://doi.org/10.1021/ma0008600>.
- [41] E. PreiB, Fracture Toughness of Freestanding Metallic Thin Films Studied by Bulge Testing, FAU University Press, 2018, <https://doi.org/10.25593/978-3-96147-118-8>.
- [42] E.I. PreiB, F. Gannott, M. Göken, B. Merle, Scaling of the fracture toughness of freestanding metallic thin films with the yield strength, *Mater. Res. Lett.* 6 (10) (Oct. 2018) 607–612, <https://doi.org/10.1080/21663831.2018.1520749>.
- [43] L. Ronan, et al., Differential tangential expansion as a mechanism for cortical gyrification, *Cereb. Cortex* 24 (8) (Aug. 2014) 2219–2228, <https://doi.org/10.1093/cercor/bht082>.
- [44] M. Vomero, et al., Achieving ultra-conformability with polyimide-based ECoG arrays, in: 2018 40th Annual International Conference of the IEEE Engineering in Medicine and Biology Society (EMBC), Jul. 2018, pp. 4464–4467, <https://doi.org/10.1109/EMBC.2018.8513171>.
- [45] C. Simitzi, A. Ranella, E. Stratakis, Controlling the morphology and outgrowth of nerve and neuroglial cells: the effect of surface topography, *Acta Biomater.* 51 (Mar. 2017) 21–52, <https://doi.org/10.1016/j.actbio.2017.01.023>.